Monthly Notices
of the
ROYAL ASTRONOMICAL SOCIETY
MNRAS **445,** 1261–1268 (2014) doi:10.1093/mnras/stu1822

The black hole–host galaxy relation for very low mass quasars

J. Sanghvi,[1]★ J. K. Kotilainen,[2] R. Falomo,[3] R. Decarli,[4] K. Karhunen[1] and M. Uslenghi[5]

[1]*Tuorla Observatory, University of Turku, Väisäläntie 20, FI-21500 Piikkiö, Finland*
[2]*Finnish Centre for Astronomy with ESO (FINCA), University of Turku, Väisäläntie 20, FI-21500 Piikkiö, Finland*
[3]*INAF – Osservatorio Astronomico di Padova, Vicolo Osservatorio 5, I-35122 Padova, Italy*
[4]*Max-Planck-Institut für Astronomie, Königstuhl 17, D-69117 Heidelberg, Germany*
[5]*INAF-IASF – via E. Bassini 15, I-20133 Milano, Italy*

Accepted 2014 September 3. Received 2014 August 13; in original form 2014 June 22

ABSTRACT

Recently, the relation between the masses of the black hole ($M_{\rm BH}$) and the host galaxy ($M_{\rm host}$) in quasars has been probed down to the parameter space of $M_{\rm BH} \sim 10^8$ M$_\odot$ and $M_{\rm host} \sim 10^{11}$ M$_\odot$ at $z < 0.5$. In this study, we have investigated the $M_{\rm BH}$–$M_{\rm host}$ log-linear relation for a sample of 37 quasars with low black hole masses (10^7 M$_\odot$ $< M_{\rm BH} < 10^{8.3}$ M$_\odot$) at $0.5 < z < 1.0$. The black hole masses were derived using virial mass estimates from Sloan Digital Sky Survey (SDSS) optical spectra. For 25 quasars, we detected the presence of the host galaxy from deep near-infrared *H*-band imaging, whereas upper limits for the host galaxy luminosity (mass) were estimated for the 12 unresolved quasars. We combined our previous studies with the results from this work to create a sample of 89 quasars at $z < 1.0$ having a large range of black hole masses (10^7 M$_\odot$ $< M_{\rm BH} < 10^{10}$ M$_\odot$) and host galaxy masses (10^{10} M$_\odot$ $< M_{\rm host} < 10^{13}$ M$_\odot$). Most of the quasars at the low-mass end lie below the extrapolation of the local relation. This apparent break in the linearity of the entire sample is due to increasing fraction of disc-dominated host galaxies in the low-mass quasars. After correcting for the disc component, and considering only the bulge component, the bilinear regression for the entire quasar sample holds over 3.5 dex in both the black hole mass and the bulge mass, and is in very good agreement with the local relation. We advocate secular evolution of discs of galaxies being responsible for the relatively strong disc domination.

Key words: galaxies: active – galaxies: bulges – galaxies: evolution – galaxies: high-redshift – galaxies: nuclei – quasars: general.

1 INTRODUCTION

Supermassive black holes (SMBHs) ubiquitously reside in the centres of massive galaxies (e.g. Kormendy & Richstone 1995; Richstone et al. 1998). However, it is still debated as to what is the mechanism that drives the formation of the black hole (BH) and how the BH is responsible for shaping the evolution of its host galaxy. A wealth of observations have shown that there is a very tight correlation between the mass of the SMBH, $M_{\rm BH}$ and the large-scale host galaxy properties, such as the stellar velocity dispersion σ_*, the luminosity of the host galaxy $L_{\rm host}$ and the mass of the host galaxy $M_{\rm host}$ (e.g. Kormendy & Richstone 1995; Ferrarese & Merritt 2000; Gebhardt 2000). This indicates a strong link between the evolution of the host galaxy and its central BH (e.g. Hopkins et al. 2007; Malbon et al. 2007; Shankar 2009 but see for e.g. Peng 2007; Jahnke & Maccio 2011 for contradicting views). In this context, accretion plays an important role by allowing the growth of BHs and thus causing the gas lying in the outskirts of the host galaxies to cool through feedback processes. This process quenches star formation. Consequently, galaxy mergers may also cause gravitationally induced dynamical instabilities, triggering bursts of star formation and gas inflows, thus fueling the BH activity (Kauffmann & Haehnelt 2000; Di Matteo, Springel & Ilernquist 2005; Canalizo et al. 2007; Bennert et al. 2008; Cisternas et al. 2011a).

Estimating the $M_{\rm BH}$ of galaxies beyond the local Universe is challenging, because the radius of influence of the BHs can be resolved only for the most nearby galaxies, whereas more distant sources require indirect tracers of $M_{\rm BH}$. Typically, the only available indirect tracer of $M_{\rm BH}$ is only applicable for type 1 AGN, based on a virial estimate of the velocity and size of the broad-line region (BLR) from the broad emission-line widths and continuum luminosity (Peterson & Wandel 2000; Vestergaard 2002; Vestergaard & Peterson 2006; Decarli et al. 2010a). This method has allowed us to estimate the $M_{\rm BH}$ from single-epoch spectra in $\sim 10^5$ quasars up to $z \sim 5$ from Sloan Digital Sky Survey (SDSS) spectra (Shen et al.

★ E-mail: jimsan@utu.fi

2011) and in additional quasars up to $z \sim 6$ (Willott, McLure & Jarvis 2003; Kurk et al. 2007; Willott et al. 2010; De Rosa et al. 2011). On the other hand, the host galaxy properties can be more easily derived from analysis of deep imaging observations.

In Decarli et al. (2010a) and Decarli et al. (2010b), we studied an extensive sample of quasars at $0 < z < 3$. Of these, 64 quasars are at $z < 1$, and most of these quasars have $M_{\rm BH} \geq 10^9$ M$_\odot$. More recently, in Decarli et al. (2012), we studied 25 quasars, most of them lying within $10^8 < M_{\rm BH}$(M$_\odot$) $< 10^9$ at $z < 0.5$, and found a large fraction of these quasars to have disc-dominated host galaxies. In Decarli et al. (2012), we showed that the linear $M_{\rm BH}$–$M_{\rm host}$ relation holds in quasars over a range of 2 dex in $M_{\rm BH}$, from 10^8 to 10^{10} M$_\odot$. For quiescent galaxies and low-luminosity AGN at low-z, $M_{\rm BH}$–$M_{\rm host}$ relation has been explored down to $M_{\rm BH} \sim 10^5$ M$_\odot$ (Greene & Ho 2007; Thornton et al. 2008; Jiang, Greene & Ho 2011a). However, little is known about the BH mass–bulge mass relation for very low mass quasars. This study extends the study of Decarli et al. (2012) by investigating the $M_{\rm BH}$–$M_{\rm host}$ mass relation down to $M_{\rm BH} \sim 10^7$ M$_\odot$ and up to $z < 1.0$.

The outline of the paper is as follows. In Section 2, we discuss how the BH masses were estimated using the virial theorem to select the samples. In Section 3, we discuss the observations, data reduction and analysis. Section 4 presents the results and discussion. In Section 5, we present the conclusions of this work.

All the work in this paper has been performed assuming the following cosmological parameters: $H_0 = 70$ km s^{-1} Mpc^{-1}, $\Omega_\Lambda = 0.7$ and $\Omega_{\rm m} = 0.3$.

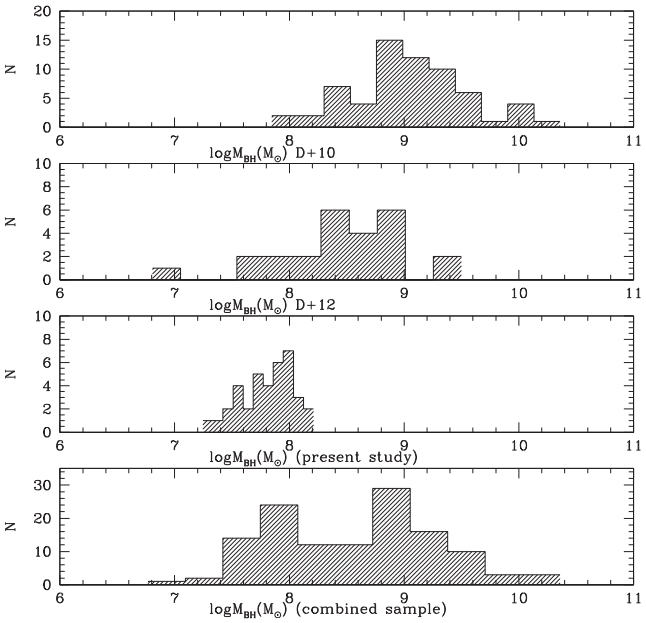

Figure 1. Comparison of the $M_{\rm BH}$ distribution of the quasars in Decarli et al. (2010a, top panel), Decarli et al. (2012, second panel) and this study (third panel). The bottom panel shows the $M_{\rm BH}$ distribution of the combined sample used in this study, emphasizing the enlarged, homogeneously covered parameter space.

2 SAMPLE SELECTION AND VIRIAL BH MASS ESTIMATION

The quasars were selected using the following criteria: (1) classification as quasars in the SDSS data base, based on optical spectra with S/N (signal-to-noise ratio) >10; (2) virial BH masses of $M_{\rm BH} < 10^{8.3}$ M$_\odot$, calculated using the Mg II emission-line width and continuum luminosity from the SDSS spectra (Shen et al. 2011), following the method described in detail in Decarli et al. (2010a); (3) the presence of at least two luminous stars within 1 arcmin projected distance from the quasar, so that the characterization of the point spread function (PSF) could be achieved with high enough precision and (4) the presence of at least two standard stars in the quasar field available in the 2MASS data base for photometric calibration. About 200 quasars fulfilled these criteria, from which the final sample of 37 quasars were selected based on observability constraints and to cover as homogeneously as possible the distribution of redshift, BH mass and quasar luminosity. Fig. 1 compares the $M_{\rm BH}$ distribution from Decarli et al. (2010a, 2012) and this work, clearly showing the extension to lower BH masses afforded by the present study.

The BH masses of the quasars, selected from the SDSS data base, were estimated using the virial theorem. To estimate the size of the BLR, we have assumed the relations between the radius of the BLR and the AGN continuum luminosity, which are calibrated using reverberation mapping results for nearby AGN (e.g. Kaspi et al. 2005; Grier et al. 2012). The continuum luminosity, together with the Mg II emission-line width contribute to provide the BH mass estimate. The spectral analysis follows as performed in Decarli et al. (2010a) and De Rosa et al. (2011). We model the AGN continuum with a power law, a Balmer pseudo-continuum and a template of the Fe II emission (Vestergaard & Wilkes 2001). Since individual features of the Fe II multiplets are typically heavily blended, we fix their width to the fitted Mg II line width. The continuum is fitted in a wide spectral region around Mg II (2500–2750 Å and 2850–3000 Å) and subtracted from the observed spectra. The Mg II line is then fitted with two Gaussian curves. The line width and the luminosities are measured from the best-fitting model. The continuum luminosity is interpolated at 3000 Å over the best-fitting power-law component. The corresponding scale radius of the BLR is computed as $R_{\rm BLR}$/(10 light days) $= (2.52 \pm 0.30)[\lambda L_\lambda(3000\,\text{Å})/(10^{44}\,\text{erg s}^{-1})]^{(0.47 \pm 0.05)}$. BH masses are thus derived as

$$M_{\rm BH} = \frac{R_{\rm BLR}(f \times \text{FWHM})^2}{G}, \quad (1)$$

where we assume $f = 1.6$ as the geometrical factor accounting for our ignorance of the BLR dynamics and orientation. The value of $f = 1.6$ is adopted in this work from Decarli et al. (2008) derived for $\langle f\text{H}(\beta)\rangle$, assuming that Mg II and H(β) emitting regions share a similar geometry (De Rosa et al. 2011).

3 IMAGING OBSERVATIONS, DATA REDUCTION AND ANALYSIS

The *H*-band imaging observations of the quasars were obtained using the 2.5 m Nordic Optical Telescope (NOT) on the Roque de los Muchachos, Spain, and the NOTCam instrument. A total of 37 quasars were observed during two observing runs in 2012 July and 2013 January. With pixel scale of 0.234 arcsec px^{-1}, NOTCam provides a total field of view of ∼4 arcmin × 4 arcmin. The average seeing during the observations was relatively good at ∼0.9 arcsec. Typical integration time was 40 min per target in 2012 July, and 63 min per target in 2013 January, as the quasars in that run were relatively fainter. A detailed summary of the observations is provided in Table 1.

Table 1. The properties of the sample and journal of observations. (1) Target name. (2) Redshift. (3) The apparent *V*-band magnitude. (4) The absolute *V*-band magnitude. (5) Estimated virial BH mass. (6) The date of imaging observation. (7) Total integration time. (8) Seeing FWHM. (9) Photometric zero-point from standard stars.

Name	z	m_v	M_v	$\log M_{BH}$ ($M_\odot$)	Date	τ (min)	FWHM (arcsec)	ZP
(1)	(2)	(3)	(4)	(5)	(6)	(7)	(8)	(9)
SDSS J013842.05+004020	0.520	19.0	−23.4	7.82	23-01-2013	42	0.91	23.13
SDSS J013912.8+152005	0.582	18.9	−23.8	7.86	24-01-2013	63	0.82	23.02
SDSS J023817.0−071810	0.605	19.3	−23.5	8.21	24-01-2013	61	0.98	22.84
SDSS J024141.52+000416	0.648	18.7	−24.3	8.15	23-01-2013	60	0.85	23.10
SDSS J074636.5+430206	0.513	18.9	−23.5	7.98	23-01-2013	63	1.45	22.91
SDSS J075517.5+152231	0.800	18.9	−24.7	8.11	23-01-2013	60	1.04	22.93
SDSS J080840.6+104738	0.714	19.0	−24.3	8.04	24-01-2013	60	0.75	22.98
SDSS J083437.0+532818	0.586	18.8	−23.9	8.02	25-01-2013	63	0.80	22.71
SDSS J091706.9+041723	0.745	19.0	−24.4	7.93	23-01-2013	63	1.10	23.10
SDSS J094838.3+184516	0.620	18.9	−24.0	7.92	24-01-2013	61	0.91	22.91
SDSS J102415.9+530019	0.892	19.3	−24.6	8.07	23-01-2013	63	0.93	22.90
SDSS J121020.7+521244	0.805	18.8	−24.8	8.02	24-01-2013	63	0.82	23.00
SDSS J124912.7+053014	0.679	18.8	−24.3	7.92	24-01-2013	63	0.84	23.00
SDSS J133401.2−024200	0.903	20.6	−23.3	7.71	23-01-2013	61	1.16	23.01
SDSS J134238.2+631347	0.539	20.5	−22.0	7.57	25-01-2013	63	1.17	23.31
SDSS J135128.15−001017	0.524	22.0	−20.5	7.54	23-01-2013	34	0.68	23.03
SDSS J135229.7+555034	0.638	20.5	−22.5	7.69	25-01-2013	63	0.70	23.00
SDSS J135501.3+015047	0.955	21.1	−23.0	7.99	24-01-2013	61	0.71	23.00
SDSS J132240.1+503011	0.780	19.9	−23.6	7.83	01-07-2012	45	0.77	22.99
SDSS J140917.5+220555	0.547	19.1	−23.5	7.96	02-07-2012	41	0.66	22.29
SDSS J145408.3+605517	0.940	20.4	−23.6	7.71	03-07-2012	45	0.68	23.06
SDSS J150518.4+022653	0.534	19.9	−22.6	7.94	01-07-2012	44	0.95	22.94
SDSS J155243.1+430605	0.860	20.4	−23.4	8.00	02-07-2012	45	1.15	22.91
SDSS J155858.2+232219	0.989	20.4	−23.7	7.88	03-07-2012	45	0.63	22.71
SDSS J160641.5+272557	0.543	20.9	−21.7	7.29	02-07-2012	41	1.40	22.86
SDSS J170134.2+254838	0.605	20.7	−22.1	7.50	03-07-2012	37	0.72	22.83
SDSS J170325.0+230001	0.566	20.4	−22.3	7.75	02-07-2012	41	0.97	22.66
SDSS J172357.0+541307	0.601	20.2	−22.6	7.68	01-07-2012	45	0.72	22.93
SDSS J173326.02+320813	0.713	20.2	−23.1	7.66	01-07-2012	54	0.70	23.10
SDSS J204443.3+010515	0.607	20.8	−22.0	7.69	01-07-2012	48	0.92	22.75
SDSS J204902.68+001803	0.510	20.7	−21.7	7.84	03-07-2012	41	0.72	23.00
SDSS J210114.99−003150	0.520	20.3	−22.1	7.46	02-07-2012	41	0.90	22.90
SDSS J210422.9−053650	0.646	19.2	−23.8	7.98	01-07-2012	54	0.84	22.90
SDSS J214138.53+000319	0.661	20.8	−22.3	7.38	02-07-2012	41	0.97	22.90
SDSS J220829.61−005024	0.750	20.7	−22.7	7.57	03-07-2012	41	0.74	22.81
SDSS J223925.9+000341	0.586	19.7	−23.1	7.57	02-07-2012	41	1.65	22.90
SDSS J234227.39−000125	0.863	19.4	−24.4	7.83	03-07-2012	36	0.94	22.50

3.1 Data reduction

Data reduction was performed using the NOTCam QUICKLOOK package based on IRAF scripts.[1] A mask file obtained from the NOTCam bad pixel mask archive was employed to mask the bad pixels in the image frames. Flat fielding was performed using a normalized median combined masterflat obtained from a pair of sky flats. For sky subtraction, a scaled sky template was produced from a list of dithered flat-fielded image frames. Finally, the flat-fielded, sky-subtracted images were aligned to within sub-pixel accuracy and combined to obtain the final reduced co-added image. Zero-point calibration was performed by cross-matching the photometry of field stars with the 2MASS data base in the *H* band.

[1] IRAF is distributed by the National Optical Astronomy Observatories, which are operated by the Association of Universities for Research in Astronomy, Inc., under cooperative agreement with the National Science Foundation.

3.2 2D image analysis

To derive the properties of the quasar host galaxies, we have used 2D model fitting of the surface brightness distribution, assuming that the image of the quasar is a superposition of the nucleus and the surrounding nebulosity. To perform this 2D data analysis, an IDL 6.0 based software package called AIDA (Astronomical Image Decomposition and Analysis; Uslenghi & Falomo 2011) was employed. The nucleus is described by the local PSF of the image and the host galaxy is modelled by a Sérsic law convolved with the PSF. Our analysis carefully follows similar modelling strategy as described in detail in Decarli et al. (2012).

3.2.1 PSF modelling

The modelling of the PSF is crucial to estimate the emission from the nuclear source against which the extended light from the host galaxy will be observed. In order to model the PSF, we employed

Table 2. Results from the image analysis. (1) Quasar name. (2) Redshift. (3) Ratio of χ^2 values between the best fit using the pure PSF model and the best fit using a PSF + galaxy model. (4) Note specifying whether the target is resolved (R), marginally resolved (M) or unresolved (U). (5) Sérsic index of the host galaxy model. (6) Apparent observed *H*-band magnitude of the nucleus. (7) Apparent observed *H*-band magnitude of the host galaxy. (8) *K*-correction between the observed *H* band and the rest-frame *R* band. (9) Resulting absolute rest-frame *R*-band magnitude of the host galaxy. (10) Adopted mass-to-light ratio. (11) Stellar mass of the host galaxy. (12) Adopted bulge luminosity to total host luminosity ratio. (13) Stellar mass of the host galaxy bulge after the disc correction.

Name	z	$\chi^2_{\rm psf}/\chi^2_{\rm gq}$	Note	$n_{\rm sersic}$	$m_{\rm nuc}$	$m_{\rm host}$	k-corr	M_R	log(M/L)	log$M_{\rm host}$ ($M_\odot$)	B/T	log$M_{\rm bulge}$ ($M_\odot$)
(1)	(2)	(3)	(4)	(5)	(6)	(7)	(8)	(9)	(10)	(11)	(12)	(13)
SDSS J013842.05+004020	0.520	1.02	M	5.00	17.44	18.94	2.56	−20.85	0.62	10.86	–	–
SDSS J013912.8+152005	0.582	1.09	M	1.06	16.89	18.81	2.54	−21.30	0.60	11.02	0.160	10.22
SDSS J023817.0−071810	0.605	1.00	U	–	16.94	>18.26	2.54	>−21.96	0.59	>11.27	–	–
SDSS J024141.52+000416	0.648	1.66	R	0.90	17.20	17.93	2.53	−22.48	0.58	11.47	0.114	10.53
SDSS J074636.5+430206	0.513	1.01	U	–	16.70	>17.82	2.57	>−21.93	0.62	>11.29	–	–
SDSS J075517.5+152231	0.800	1.01	U	–	16.19	>17.50	2.48	>−23.52	0.54	>11.85	–	–
SDSS J080840.6+104738	0.714	1.01	U	–	17.54	>18.19	2.51	>−22.49	0.56	>11.46	–	–
SDSS J083437.0+532818	0.586	1.52	R	2.65	16.93	17.80	2.54	−22.32	0.60	11.43	0.614	11.22
SDSS J091706.9+041723	0.745	1.00	U	–	18.51	>18.31	2.50	>−22.50	0.55	>11.45	–	–
SDSS J094838.3+184516	0.620	1.00	U	–	16.54	>17.82	2.53	>−22.47	0.59	>11.48	–	–
SDSS J102415.9+530019	0.892	1.10	R	2.33	17.35	18.46	2.46	−22.86	0.51	11.56	0.522	11.27
SDSS J121020.7+521244	0.805	1.40	R	0.90	17.04	18.30	2.48	−22.73	0.53	11.52	0.114	10.58
SDSS J124912.7+053014	0.679	1.05	M	0.90	16.78	19.09	2.52	−21.44	0.57	11.05	0.114	10.11
SDSS J132240.1+503011	0.780	1.02	M	2.16	18.42	19.13	2.49	−21.80	0.54	11.16	0.474	10.84
SDSS J133401.2−024200	0.903	0.89	U	–	18.63	>18.82	2.46	>−22.54	0.51	>11.43	–	–
SDSS J134238.2+631347	0.539	1.16	R	0.90	18.75	19.15	2.56	−20.74	0.61	10.81	0.114	9.86
SDSS J135128.15−001017	0.524	4.91	R	4.16	19.79	16.48	2.56	−23.34	0.62	11.86	–	–
SDSS J135229.7+555034	0.638	1.13	R	0.90	18.34	18.95	2.53	−21.41	0.59	11.06	0.114	10.11
SDSS J135501.3+015047	0.955	1.67	R	1.07	19.42	18.12	2.44	−23.40	0.50	11.76	0.162	10.97
SDSS J140917.5+220555	0.547	1.15	R	5.00	16.42	17.83	2.56	−22.10	0.61	11.35	–	–
SDSS J145408.3+605517	0.940	1.02	U	–	18.06	>18.93	2.44	>−22.56	0.50	>11.42	–	–
SDSS J150518.4+022653	0.534	1.01	U	–	17.29	>17.93	2.56	>−21.94	0.61	>11.29	–	–
SDSS J155243.1+430605	0.860	1.00	U	–	17.92	>18.69	2.47	>−22.53	0.52	>11.43	–	–
SDSS J155858.2+232219	0.989	1.01	U	–	18.07	>19.07	2.43	>−22.57	0.49	>11.42	–	–
SDSS J160641.5+272557	0.543	1.15	R	0.90	17.70	17.84	2.56	−22.06	0.61	11.34	0.114	10.39
SDSS J170134.2+254838	0.605	1.13	R	1.29	18.77	18.39	2.54	−21.82	0.59	11.22	0.225	10.57
SDSS J170325.0+230001	0.566	1.04	R	0.90	18.08	18.60	2.55	−21.43	0.60	11.07	0.114	10.13
SDSS J172357.0+541307	0.601	1.03	R	0.90	18.15	19.66	2.54	−20.53	0.60	10.71	0.114	9.77
SDSS J173326.02+320813	0.713	1.06	R	5.00	18.52	18.78	2.51	−21.89	0.56	11.22	–	–
SDSS J204443.3+010515	0.607	1.64	R	0.90	19.10	17.43	2.53	−22.80	0.59	11.61	0.114	10.67
SDSS J204902.68+001803	0.510	1.42	R	5.00	19.10	17.76	2.57	−21.97	0.62	11.31	–	–
SDSS J210114.99−003150	0.520	1.24	R	0.90	18.64	18.32	2.56	−21.47	0.62	11.11	0.114	10.17
SDSS J210422.9−053650	0.646	2.86	R	1.97	18.37	17.05	2.53	−23.34	0.58	11.82	0.420	11.44
SDSS J214138.53+000319	0.661	1.02	R	0.90	19.71	19.60	2.52	−20.87	0.58	10.83	0.114	9.88
SDSS J220829.61−005024	0.750	1.13	R	5.00	18.30	18.30	2.50	−22.52	0.55	11.46	–	–
SDSS J223925.9+000341	0.586	1.03	U	–	17.23	>18.17	2.54	>−21.96	0.60	>11.28	–	–
SDSS J234227.39−000125	0.863	1.04	R	0.90	17.78	18.75	2.47	−22.48	0.52	11.41	0.114	10.47

multiple field stars within the frame of each quasar, that were bright enough to model the faint PSF wing. For the selection of the field stars, we preferentially chose stars with the smallest full width at half-maximum (FWHM) and ellipticity and having brightest magnitude in the field. Contamination near the regions close to the stars, including companions, saturated pixels or other defects were carefully masked out. The selected stars were each modelled with four 2D Gaussians and an exponential feature. The Gaussians and the exponential feature represented the core of the PSF and the extended PSF wings, respectively. A circular annulus centred around the stars was used to calculate the local background. The final PSF fit region was selected after defining the internal and external radius of the circular area. This allowed us to remove the cores of bright, saturated stars. Typical uncertainty in the PSF model is $\leq\sim$0.3 mag. For a detailed discussion on the PSF characterization, see Kotilainen et al. (2007, 2009).

3.2.2 *Host characterization*

After modelling the PSF, in order to distinguish between the resolved and unresolved quasars, the images of the quasars were first fitted with a pure PSF model. If there was extended emission observed in the residuals or if the residuals showed a significant excess over the PSF shape, in a region relatively far away from the nucleus (typically between 1 and 2 arcsec), then we considered the quasar to be resolved. The resolved quasars were further fitted with a two component (PSF + galaxy) model. The fitting was performed using the Sérsic model convolved with the PSF to describe the host galaxy and a scaled PSF to describe the nucleus. To evaluate whether the quasar is resolved, marginally resolved or unresolved, we investigated the χ^2 ratio of the fits (see Table 2), statistically providing the amount of deviation of the PSF + galaxy model from the pure PSF fit. For a resolved quasar, the PSF + galaxy model is expected to be better than the pure PSF fit. In most cases, the ratio is above 1.1

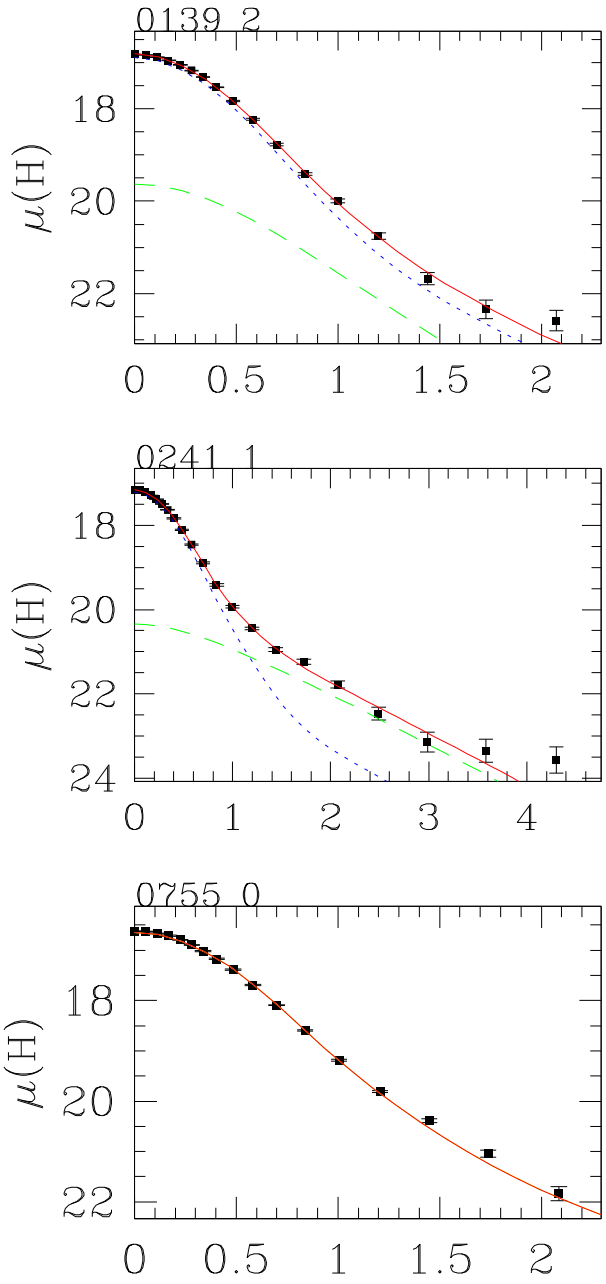

Figure 2. Profiles of *H*-band radial surface brightness versus radius in arcsec, are shown for three QSOs (from top to bottom – SDSS J013912.8+152005, SDSS J024141.52+000416, SDSS J075517.5+152231), overlaid with scaled PSF model (blue, dotted line), the de Vaucouleurs $r^{1/4}$ model convolved with the PSF (green, long dashed line) and the fitted PSF+host galaxy model profile (red, solid line). From top to bottom, they are classified as Marginally resolved, Resolved and Unresolved case. For a complete list of such profiles of all the quasars in this study, please refer the online electronic version of this paper.

for resolved quasars, around 1 for unresolved quasars and between these values for the marginally resolved quasars. In some exceptional cases, the values represented by the χ^2 ratio are not sufficient to characterize whether the quasar is resolved or not. Therefore, we conducted additional visual inspection of the profiles, examples of which are shown in Fig. 2, to robustly ascertain whether the PSF + galaxy fit was better than the pure PSF fit. For the unresolved quasars, we visually determined the upper limit to their host galaxy luminosity by adding increasingly bright galaxy models to the PSF model, up to the point where the model profile became inconsistent with the observed profile within the observational error bars. There are four quasars which fit neither the resolved, nor the unresolved class, and we classify them as marginally resolved cases. An example of the output of this analysis is shown in Fig. 2. For a detailed discussion on the host galaxy characterization, see Kotilainen et al. (2007, 2009).

In Table 2, it can be seen that the Sérsic index n_s for a large fraction of the quasars tends to be either 0.90 or 5.00, the extreme values considered by the AIDA pipeline. However, Table 2 shows also that 50 per cent of the marginally resolved quasars have well-defined (i.e. not extreme) Sérsic index values, indicating that there are no systematic errors. We also note that n_s does not show inverse correlation with the effective radius, as would be expected if the pipeline were erroneously identifying a PSF with broad wings as a small bulge.

The 2D model fitting with AIDA provides us with the apparent host galaxy magnitudes in the *H* band. These apparent magnitudes were converted to the rest-frame *R*-band absolute magnitudes, using the elliptical galaxy template from Mannucci et al. (2001) to estimate the required *K*-correction. Then the *R*-band absolute magnitudes of the host galaxies were converted into stellar mass, assuming the mass-to-light (M/L) ratio of a single-stellar population originating at $z_{\rm burst} = 5$ and passively evolving down to $z = 0$ (Decarli et al. 2010b).

3.2.3 *Error estimation*

The errors associated with the parameters of the best fit depend on a number of assumptions based on the effective observing conditions (e.g. for the residual uncertainty of the background subtraction which particularly affects near-IR images) that are not always well understood. Moreover, a number of systematic effects can further introduce uncertainties. The best way to estimate the uncertainties of the fitting parameters is to produce simulated images of the objects to try to achieve similar parameters and conditions, as those from real observations and thereby to evaluate the uncertainty of a given parameter by analysing multiple mock observations. In order to perform such a test for each object, we produced simulated images of the targets assuming the best-fitting parameters and the noise level derived from the real observations. The instrumental setup was fixed by the values of pixel scale, read-out noise, gain, exposure time, number of combined exposures and the zero-point of the calibration. The simulated images were produced using the Advanced Exposure Time Calculator (AETC; Falomo, Fantinel & Uslenghi 2011) tool[2] and then analysed with AIDA using the same conditions adopted for the analysis of the real images but not using information about the true parameters of the target. For each target, we performed 25 simulations and then compared the distribution of the parameters with those derived from the best fit of the real data. It turned out that the total magnitude of the objects always lies within a few millimagnitudes, whereas for the host galaxy magnitude the typical uncertainty ranges from 0.2 mag for well-resolved sources to 0.6–0.8 mag for the marginally resolved sources. We also report that the uncertainties in the effective radius for well-resolved objects are within 20–30 per cent in most cases, while for marginally resolved objects the uncertainty can be as high as 80 per cent. The most critical parameter is the index n_s of the Sérsic model.

[2] AETC – Advanced Exposure Time Calculator: http://aetc.oapd.inaf.it/

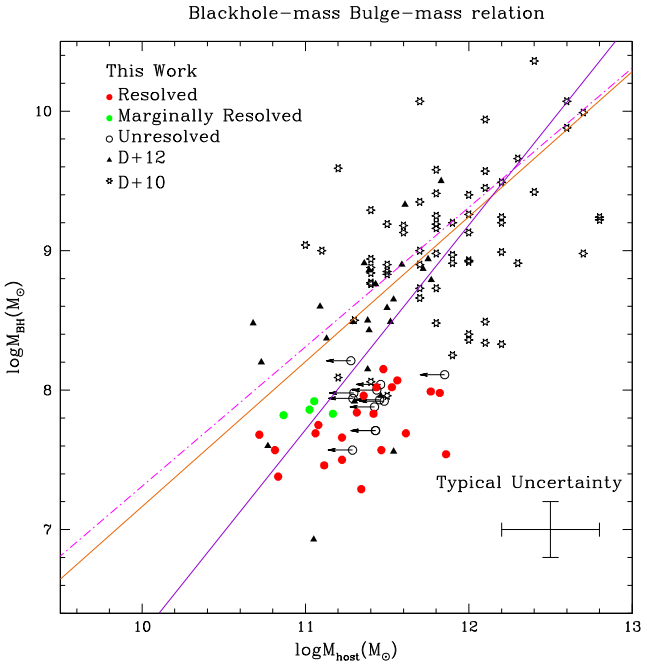

Figure 3. The $M_{\rm BH}$–$M_{\rm host}$ relation for quasars in this work (red circles: resolved, green circles: marginally resolved and open circles: unresolved), Decarli et al. (2010a) and Decarli et al. (2010b, open stars) and Decarli et al. (2012, black triangles). The best bilinear regression fit is shown for the entire resolved sample (violet solid line) and for the quasars with $\log M_{\rm BH} > 8.2\,{\rm M}_{\odot}$ (dark orange solid line). The regression fit for the local relation for inactive galaxies by Marconi & Hunt (2003) is shown as magenta dashed line, with $\langle\Gamma\rangle \sim 0.002$. A typical error bar is shown in the lower right corner.

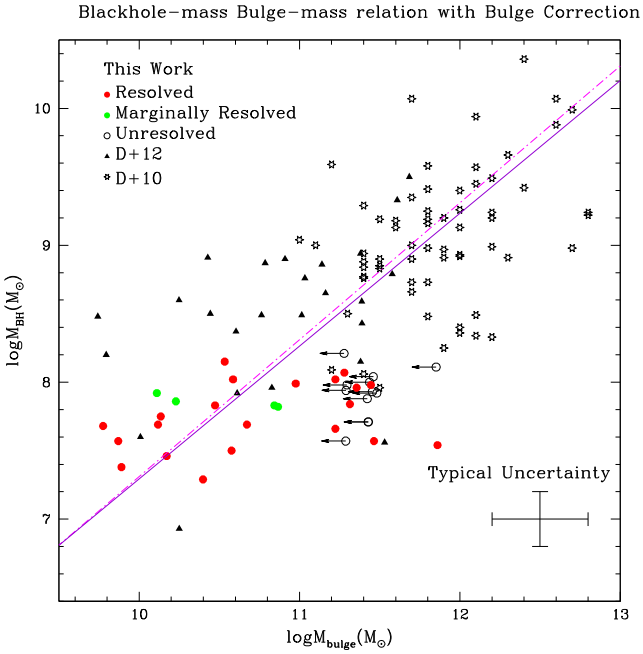

Figure 4. The $M_{\rm BH}$–$M_{\rm bulge}$ relation after the disc correction. The best bilinear regression fit is shown for the entire resolved sample as violet solid line while the magenta dashed line shows the regression fit for the local relation for inactive galaxies by Marconi & Hunt (2003) with $\langle\Gamma\rangle \sim 0.002$. For meaning of symbols, see Fig. 3 caption.

4 RESULTS AND DISCUSSIONS

Out of our sample of 37 quasars with low-mass BHs, 21 (57 per cent) are resolved, 4 (11 per cent) are marginally resolved and 12 (32 per cent) remain unresolved. We have produced the full quasar sample with BH masses up to $M_{\rm BH} \leq 10^{10}\,{\rm M}_{\odot}$ by including all the quasars at $z < 1$ from Decarli et al. (2010a,b, 2012). The $M_{\rm BH}$–$M_{\rm host}$ relation up to z <1.0 is shown in Fig. 3. As can be seen, the full quasar sample defines a linear relation. However, the quasars with $M_{\rm BH} < 10^{8}\,{\rm M}_{\odot}$ deviate from the relation defined by the quasars at $M_{\rm BH} > 10^{8.2}\,{\rm M}_{\odot}$ and the local relation (Marconi & Hunt 2003). The $M_{\rm BH}$–$M_{\rm host}$ relation becomes indeed steeper and slightly tighter at the lowest BH masses, causing the linear relation to apparently break down at $M_{\rm BH} \sim 10^{8.2}\,{\rm M}_{\odot}$. The best bilinear regression fits of the entire sample of resolved quasars (equation 2) and for resolved quasars with $M_{\rm BH} > 10^{8.2}\,{\rm M}_{\odot}$ (equation 3) are given as

$$\log\frac{M_{\rm BH}}{10^{8.5}\,{\rm M}_{\odot}} = (1.46 \pm 0.25) \times \log\frac{M_{\rm host}}{10^{11.7}\,{\rm M}_{\odot}} + (0.24 \pm 0.11) \quad (2)$$

$$\log\frac{M_{\rm BH}}{10^{8.5}\,{\rm M}_{\odot}} = (1.03 \pm 0.24) \times \log\frac{M_{\rm host}}{10^{11.7}\,{\rm M}_{\odot}} + (0.43 \pm 0.10). \quad (3)$$

Such a break in the relation could in principle be caused by a systematic (a) underestimation of $M_{\rm BH}$ and/or (b) overestimation of $M_{\rm host}$, at low BH masses. We believe that neither explanation is likely, as (a) BH masses based on SDSS spectra have been shown to be robust in numerous previous studies (e.g. Labita et al. 2009; Rafiee & Hall 2011), and the amount of uncertainty required to explain the break is much higher than the expected uncertainty in deriving $M_{\rm BH}$. As for case (b), the majority of our sample quasars are well resolved, leading to a robust determination of the host galaxy luminosity/mass (e.g. Falomo et al. 2014). In addition, the amount of systematic error would require an order of magnitude underestimation of the PSF model. Hence, the most likely reason for the apparent break in the $M_{\rm BH}$–$M_{\rm host}$ relation below $M_{\rm BH} \sim 10^{8.2}\,{\rm M}_{\odot}$ is due to significant disc contamination.

Disc correction was therefore performed for quasars having disc components because bulge mass is better correlated with $M_{\rm BH}$ than the disc mass or the total host galaxy mass. Due to the seeing-limited spatial resolution of ground-based observations, accurate decomposition of quasar host galaxies at high-z into bulge and disc components is practically impossible. However, the Sérsic index $n_{\rm s}$ can be used to estimate the galaxy morphology such that, $n_{\rm s} \sim 1$ indicates disc-dominated galaxies whereas, $n_{\rm s} \sim 4$ indicates elliptical galaxies. Simard et al. (2011) performed bulge-disc decomposition of $\sim 10^{6}$ galaxies from the SDSS by analytical estimation. Decarli et al. (2012) followed similar analytical approach which is also adopted in this work, for correcting the disc component.

$$\frac{B}{T} = \frac{n_{\rm s} - 0.5}{3.5} \quad (4)$$

for $n_{\rm s} < 4$.

The above analytical equation for disc correction can be used to estimate a range of $\frac{B}{T}$ values for $n_{\rm s} < 4$. No disc correction is required for $n_{\rm s} \geq 4$, i.e. pure spheroidal galaxies. Fig. 4 shows the $M_{\rm BH}$–$M_{\rm bulge}$ relation after performing the disc correction. A detailed summary of our results is shown in Table 2. The best bilinear regression fit of the $M_{\rm BH}$–$M_{\rm bulge}$ relation (after disc correction), considering all the

resolved quasar samples is given as

$$\log\frac{M_{\rm BH}}{10^{8.5}\,{\rm M}_{\odot}} = (0.97 \pm 0.15) \times \log\frac{M_{\rm host}}{10^{11.7}\,{\rm M}_{\odot}} + (0.44 \pm 0.11). \quad (5)$$

The slope of the relation becomes indeed flatter than the slope of the relation without disc correction. After correcting for the disc contamination, the best fit of the relation is in very good agreement with the local relation, indicating that the apparent break in the regression fit is caused by disc-dominated galaxies.

It is evident from Fig. 4 that the quasars from Decarli et al. (2012) corrected for the disc contamination are in similar mass scales in $M_{\rm bulge}$ as our disc-corrected quasars. The overall scatter of the relation does not change significantly after the disc correction. Consecutively, $\langle\log\Gamma\rangle(\equiv\frac{M_{\rm BH}}{M_{\rm host}})$ increases from -2.98 ± 0.0511 to -2.74 ± 0.0536. It is worth to note that this study extends the parameter space of the disc-corrected relation up to ∼3.5 dex in both $M_{\rm BH}$ and $M_{\rm bulge}$ towards the low-mass end.

Galaxies can be classified based on their surface brightness profiles as core-Sérsic galaxies (typically massive and luminous having undergone dry mergers) and Sérsic galaxies (typically less massive; $M_{\rm host} \leq 3 \times 10^{10}\,{\rm M}_{\odot}$). Scott, Graham & Schombert (2013) found the best bilinear regression fits for nearby core-Sérsic and Sérsic galaxies as $M_{\rm BH} \propto M_{\rm host}^{0.80}$ and $M_{\rm BH} \propto M_{\rm host}^{1.80}$, respectively. This study includes eight resolved quasars that can be classified as Sérsic galaxies. Furthermore, 62 quasars from Decarli et al. (2010a) and Decarli et al. (2010b) and 18 quasars from Decarli et al. (2012) can be classified as purely core-Sérsic galaxies and three quasars as purely Sérsic galaxies. It is worth to mention that for our quasars with disc dominated host galaxies, their bulge masses are considered. The bilinear regression for core-Sérsic and Sérsic galaxies in this study up to $z < 1$ extending into the low-mass region are given as $M_{\rm BH} \propto M_{\rm host}^{0.80}$ and $M_{\rm BH} \propto M_{\rm host}^{1.22}$, respectively.

In accordance with the morphological analysis and the bulge + disc decomposition performed in this work, we find that ∼3/4 of all the resolved and marginally resolved quasars possess significant disc components. Since most of these quasars lie below the local relation, we can infer that, for these bulges to increase and fit themselves with the local relation, a mechanism is required that would redistribute the stellar content of the galaxy. Such a scenario has already been encountered in the previous low-mass quasar studies, e.g. Cisternas et al. (2011b), Schramm & Silverman (2013) and Decarli et al. (2012). This makes it vital to correct the host galaxy masses for the disc component, to consider the bulge component only. Recently, Kormendy, Bender & Cornell (2011) and Sani et al. (2011) have suggested that galaxies that lie below the log-linear $M_{\rm BH}$–$M_{\rm host}$ mass relation of inactive galaxies, are evidently pseudo-bulges. On the contrary, Graham (2012) argues that galaxies hosting low-mass SMBHs are not pseudo-bulges, but rather an overlooked case of non-log-linear nature of $M_{\rm BH}$–$M_{\rm host}$ relation for classical spheroids. Although the relation for the Sérsic galaxies in our study is steeper than for the core-Sérsic galaxies, as seen in the previous discussion, we do not find evidence for a 'break' in the slope, as advocated by Graham (2012) and Scott et al. (2013), as we find that a single log-linear relation is recovered after the disc correction. The secular evolution of galaxy discs can allow the stars and gas within the galaxy to redistribute themselves in response to instabilities. In that case, mergers are not a likely scenario responsible for the stellar redistribution in the discs. Similarly, Jiang et al. (2011b) found for a sample of 147 nearby active galaxies with $M_{\rm BH}$ ranging between 10^5 and $10^6\,{\rm M}_{\odot}$ that a higher fraction of galaxies were disc-dominated likely containing pseudo-bulges, evolving secularly. Our results are consistent with those by Kormendy et al. (2011) and Kormendy & Bender (2011), who found that high-mass pseudo-bulges with $M_{\rm BH} > 10^7\,{\rm M}_{\odot}$ follow the $M_{\rm BH}$–$M_{\rm host}$ correlation. Only at lower masses, which our quasar samples do not probe, the pseudo-bulges start to deviate from the BH–host correlation.

Decarli et al. (2010b) found evidence for strong evolution in Γ in their large sample of high-mass quasars, increasing by a factor ∼2 from $z = 0$ to $z = 1$ ($\log\Gamma$ increases from −2.91 to −2.63). At lower masses, we find that the $\langle\log\Gamma\rangle$, considering the bulge component (i.e. disc-corrected galaxy masses), evolves from $\log\Gamma \sim -2.39 \pm 0.12$ at $\langle z\rangle = 0.286$ in Decarli et al. (2012) to $\log\Gamma \sim -2.98 \pm 0.12$ at $\langle z\rangle = 0.653$ in this work, i.e. a decrease in Γ by a factor ∼3.5. There is, however, a marked difference in the $M_{\rm BH}$ distribution of the samples, so it is not possible to ascertain how much of the observed evolution, if any, is due to real redshift evolution.

5 CONCLUSIONS

The $M_{\rm BH}$ and host galaxy properties of a sample of 37 low-mass quasars were combined with 89 quasars from the literature up to $z < 1.0$ and up to $M_{\rm BH} < 10^{11}\,{\rm M}_{\odot}$, to investigate the relationship between BH-mass ($M_{\rm BH}$) and host galaxy mass ($M_{\rm host}$). From this study we conclude that:

(1) There is an apparent break at $M_{\rm BH} \sim 10^{8.2}\,{\rm M}_{\odot}$ in the $M_{\rm BH}$–$M_{\rm host}$ relation.

(2) The host galaxies of ∼75 per cent of the quasars in our sample of low-mass quasars is dominated by a disc component.

(3) After correcting for the disc component, the linear $M_{\rm BH}$–$M_{\rm bulge}$ relation holds over the entire parameter space [$(10^{6.9}$–$10^{10.4} M_{\rm BH}({\rm M}_{\odot})) \sim 3.5$ dex for $M_{\rm BH}$ and $(10^{9.5}$–$10^{13} M_{\rm bulge}({\rm M}_{\odot}))$∼3.5 dex for $M_{\rm bulge}$].

(4) The $M_{\rm BH}$– $M_{\rm bulge}$ relation is in very good agreement with the local relation after disc correction.

(5) We discuss the scenario of secular evolution of discs of galaxies being responsible for the relatively strong disc domination.

ACKNOWLEDGEMENTS

All the authors are grateful to the anonymous referee for the inquisitive review and time, which improvised the paper.

Funding for the SDSS and SDSS-II has been provided by the Alfred P. Sloan Foundation, the Participating Institutions, the National Science Foundation, the U.S. Department of Energy, the National Aeronautics and Space Administration, the Japanese Monbukagakusho, the Max Planck Society, and the Higher Education Funding Council for England. The SDSS Web Site is http://www.sdss.org/.

The SDSS is managed by the Astrophysical Research Consortium for the Participating Institutions. The Participating Institutions are the American Museum of Natural History, Astrophysical Institute Potsdam, University of Basel, University of Cambridge, Case Western Reserve University, University of Chicago, Drexel University, Fermilab, the Institute for Advanced Study, the Japan Participation Group, Johns Hopkins University, the Joint Institute for Nuclear Astrophysics, the Kavli Institute for Particle Astrophysics and Cosmology, the Korean Scientist Group, the Chinese Academy of Sciences (LAMOST), Los Alamos National Laboratory, the Max-Planck-Institute for Astronomy (MPIA), the Max-Planck-Institute for Astrophysics (MPA), New Mexico State

University, Ohio State University, University of Pittsburgh, University of Portsmouth, Princeton University, the United States Naval Observatory, and the University of Washington.

J.S. acknowledges and is grateful for the financial support by Vilho, Yrjö and Kalle Väisälä Foundation provided in 2014.

Based on observations made with the NOT, operated by the NOT Scientific Association at the Observatorio del Roque de los Muchachos, La Palma, Spain, of the Instituto de Astrofisica de Canarias.

REFERENCES

Bennert N., Canalizo G., Jungwiert B., Stockton A., Schweizer F., Peng C. Y., Lacy M., 2008, ApJ, 677, 846
Canalizo G., Bennert N., Jungwiert B., Stockton A., Schweizer F., Lacy M., Peng C., 2007, ApJ, 669, 801
Cisternas M. et al., 2011a, ApJ, 726, L57
Cisternas M. et al., 2011b, ApJ, 741, L11
De Rosa G., Decarli R., Walter F., Fan X., Jiang L., Kurk J., Pasquali A., Rix H. W., 2011, ApJ, 739, 56
Decarli R., Labita M., Treves A., Falomo R., 2008, MNRAS, 387, 1237
Decarli R., Falomo R., Treves A., Kotilainen J. K., Labita M., Scarpa R., 2010a, MNRAS, 402, 2441
Decarli R., Falomo R., Treves A., Labita M., Kotilainen J. K., Scarpa R., 2010b, MNRAS, 402, 2453
Decarli R., Falomo R., Kotilainen J., Hyvönen T., Uslenghi M., Treves A., 2012, Adv. Astron., 2012, 782528
Di Matteo T., Springel V., Hernquist L., 2005, Nature, 433, 7026, 604
Falomo R., Fantinel D., Uslenghi M., 2011, in Tescher A. G., ed., Proc. SPIE Conf. Ser. Vol. 8135, Applications of Digital Image Processing XXXIV. SPIE, Bellingham, p. 813523
Falomo R., Bettoni D., Karhunen K., Kotilainen J. K., Uslenghi M., 2014, MNRAS, 440, 476
Ferrarese L., Merritt D., 2000, ApJ, 539, L9
Gebhardt K. et al., 2000, ApJ, 539, L13
Graham A. W., 2012, ApJ, 746, 113
Greene J. E., Ho L. C., 2007, ApJ, 670, L92
Grier C. J. et al., 2012, ApJ, 755, 60
Hopkins P. F., Hernquist L., Cox T. J., Robertson B., Krause E., 2007, ApJ, 669, 45
Jahnke K., Maccio A., 2011, ApJ, 734, 92
Jiang Y. F., Greene J. E., Ho L. C., 2011a, ApJ, 737, L45
Jiang Y. F., Greene J. E., Ho L. C., Xiao T., Barth A. J., 2011b, ApJ, 742, 68
Kaspi S., Maoz D., Netzer H., Peterson B. M., Vestergaard M., Jannuzi B. T., 2005, ApJ, 629, 61
Kauffmann G., Haehnelt M., 2000, MNRAS, 311, 576
Kormendy J., Bender R., 2011, Nature, 469, 377
Kormendy J., Richstone D., 1995, ARA&A, 33, 581
Kormendy J., Bender R., Cornell M., 2011, Nature, 469, 374
Kotilainen J. K., Falomo R., Labita M., Treves A., Uslenghi M., 2007, ApJ, 660, 1039
Kotilainen J. K., Falomo R., Decarli R., Treves A., Uslenghi M., Scarpa R., 2009, ApJ, 703, 1663
Kurk J. D. et al., 2007, ApJ, 669, 32
Labita M., Decarli R., Treves A., Falomo R., 2009, MNRAS, 399, 2099
Malbon R. K., Baugh C. M., Frenk C. S., Lacey C. G., 2007, MNRAS, 382, 1394
Mannucci F., Basile F., Poggianti B. M., Cimatti A., Daddi E., Pozzetti L., Vanzi L., 2001, MNRAS, 326, 745
Marconi A., Hunt L. K., 2003, ApJ, 589, L21
Peng C. Y., 2007, ApJ, 671, 1098
Peterson B. M., Wandel A., 2000, ApJ, 540, L13
Rafiee A., Hall P. B., 2011, ApJS, 194, 42
Richstone D. et al., 1998, Nature, 395, A14
Sani E., Marconi A., Hunt L., Risaliti G., 2011, MNRAS, 413, 1479
Schramm M., Silverman J. D., 2013, ApJ, 767, 13
Scott N., Graham A. W., Schombert J., 2013, ApJ, 768, 76
Shankar F., 2009, New Astron. Rev., 53, 57
Shen Y. et al., 2011, ApJS, 194, 45
Simard L. J., Mendel T., Patton D. R., Ellison S. L., McConnachie A. W., 2011, ApJS, 196, 11
Thornton C. E., Barth A. J., Ho L. C., Rutledge R. E., Greene J. E., 2008, ApJ, 686, 892
Uslenghi M., Falomo R., 2011, in Tescher A. G., ed., Proc. SPIE Conf. Ser. Vol. 8135, AIDA: A Software Package For 2D Model Fitting Analysis of Astronomical Images. SPIE, Bellingham, p. 813524
Vestergaard M., 2002, ApJ, 571, 733
Vestergaard M., Peterson B. M., 2006, ApJ, 641, 689
Vestergaard M., Wilkes B., 2001, ApJS, 134, 1
Willott C. J., McLure R. J., Jarvis M. J., 2003, ApJ, 587, L15
Willott C. J. et al., 2010, AJ, 140, 546

SUPPORTING INFORMATION

Additional Supporting Information may be found in the online version of this article:

Figure 2. Profiles of *H*-band radial surface brightness versus radius in arcsec, are shown for three QSOs (from top to bottom – SDSS J013912.8+152005, SDSS J024141.52+000416, SDSS J075517.5+152231), overlaid with scaled PSF model (blue, dotted line), the de Vaucouleurs $r^{1/4}$ model convolved with the PSF (green, long dashed line) and the fitted PSF+host galaxy model profile (red, solid line) (http://mnras.oxfordjournals.org/lookup/suppl/doi:10.1093/mnras/stu1822/-/DC1).

Please note: Oxford University Press are not responsible for the content or functionality of any supporting materials supplied by the authors. Any queries (other than missing material) should be directed to the corresponding author for the paper.

This paper has been typeset from a TEX/LATEX file prepared by the author.